Ancillary Services Provided by Photovoltaic Inverters: Single and Three Phase Control Strategies

A. F. Cupertino, H. A. Pereira and L. S. Xavier

Ancillary Services Provided by Photovoltaic Inverters: Single and Three Phase Control Strategies

Lucas S. Xavier [1], Allan F. Cupertino [2], Heverton A. Pereira[3]

[1] Department of Electrical Engineering, Federal University of Minas Gerais, Av. Pres. Antônio Carlos, 6627 Belo Horizonte, MG, Brazil

[2] Department of Materials Engineering, Federal Center for Technological Education of Minas Gerais, Av. Amazonas 5253, 30421-169, Belo Horizonte - MG, Brazil

[3] Department of Electrical Engineering, Federal University of Viçosa, Av. P. H. Rolfs s/n, 36570-900, Viçosa - MG, Brazil

e-mail: lucas.xavier@ufv.br, allan.cupertino@yahoo.com.br, heverton.pereira@ufv.br

Abstract: Grid connected photovoltaic (PV) have been inserted in the power systems mainly at low and medium voltage. PV inverters are power electronic based converters with fast response in the range of milliseconds. Besides, due to solar irradiance variation, these converters have excess capacity that can be used to provide ancillary services to the main grid. Traditionally, ancillary services such as reactive power injection and frequency support are provided by hydro and thermal generation. This work is focused on the analysis of how PV inverters can perform ancillary services and support the grid. Control strategies for reactive power injection and harmonic current compensation are explored. Furthermore, the inverter current saturation plays an important role, once high currents can damage the inverter or reduce its lifetime. Case studies for single and three-phase PV inverters are presented. It is observed that the ancillary service priority must be defined in order to guarantee PV inverter operation under nominal conditions.
Keywords: Ancillary services; PV inverter; Reactive Power Injection; Harmonic current compensation.

1. Introduction

In grid-connected photovoltaic (PV) system, there is a based power electronic converter, that injects direct current (dc) from PV panels into the alternating current (ac) grid. This electronic converter, known as inverter, can be connected to single-phase or three-phase power systems [1], [2]. The single-phase PV inverters are commonly used for applications up to 7 kW. Above this value, three-phase inverters are usually recommended for ensuring a better electric power balance among the phases.

In most applications, single-phase and three-phase photovoltaic inverters extract the PV panel energy and inject it into the grid, with unitary power factor. Due to solar irradiance variation during the day, the solar inverters have an operation margin, in terms of current, which is not used over the PV system daily operation [3]. Fig. 1 (a) is defined as the maximal injected power of an inverter, and Fig. 1 (b) shows an operation curve of a real PV plant during a typical sunny day. It is possible to note that the operation curve does not exceed 30 % of the total operation area. Thereby, it remains an area of 70 %, which can be used for ancillary services, as illustrated in Fig. 1 (c).

The most common ancillary services required by the Operation Systems are reactive power injection and frequency support. Furthermore, a maximal current harmonic distortion is allowed, depending on the voltage level at the Point of Common Coupling (PCC). These ancillary services supported by PV systems have been discussed in recent years, given the importance of taking advantage of the PV system excess capacity.
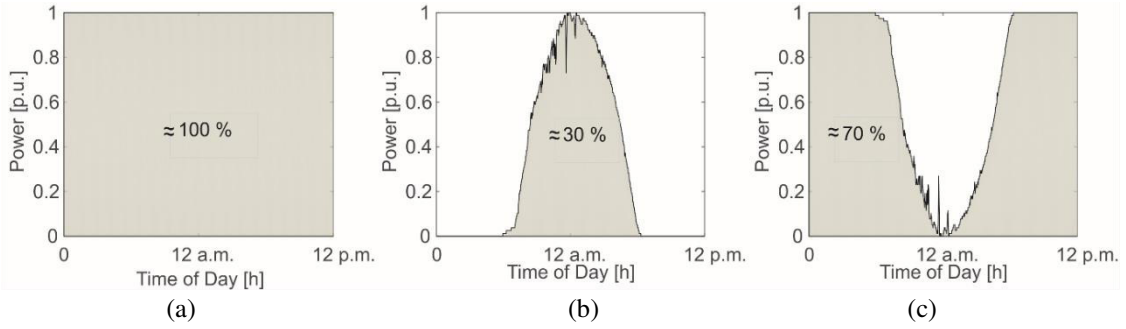
Fig. 1. Operation curve of a real PV system during an operation day. (a) Operation total area during one day. (b) Operation curve of a real PV plant during a measurement day. (c) Available operation area for ancillary services.

Several control challenges are associated when the PV systems are used to perform ancillary services in order to improve the grid power quality. For example, in harmonic compensation, it is important to detect the current or voltage harmonic information. In references [4], [5] and [6] it is used the method based on conservative power theory to detect the harmonic current of the load. On the other hand, in [7] is used the PCC voltage information for harmonic compensation through a voltage control loop. Furthermore, the PV inverter has a current limitation which cannot be exceeded. For this reason, it is important to design the strategy to limit the inverter current during ancillary service operation, ensuring the rated current below the reference. The determination of a current limit is relatively simple for reactive power compensation. However, when harmonic current compensation is involved, it is very difficult to calculate the inverter current peak by an analytical expression [3], [4].

In view of the above discussions, the contribution of this work is to present an overview of ancillary services provided by PV systems with focuses on reactive power and harmonic current compensation. Several control strategies in different reference frames are presented for single-phase and three-phase systems, including partial compensation. Additionally, computational simulation results are included to show the performance of the PV single-phase and three-phase system during reactive power and harmonic current compensation. This work brings a theoretical basis of control strategies applied to photovoltaic converters performing reactive power and harmonic current compensation.

This paper has an overview of the PV system structures in Section 2 and an overview of the main ancillary services that the PV systems can provide in Section 3. In Section 4, several control schemes for PV inverter including the capability to perform reactive power injection and harmonic current compensation are described. In Section 5, the inverter current controller and strategies for partial compensation of the reactive power and harmonic current are explored. Section 6 describes the parameters used in the case study, and Section 7 shows the main results for both single and three-phase PV inverters during reactive power injection and harmonic current compensation. Finally, conclusions are stated in Section 8.

2. Conventional Structure of PV Systems

The aim of this section is to provide a brief overview of the conventional structure of PV systems. A generic topology of a grid connected PV system is shown in Fig. 2. The dc/dc stage is commonly used in single-phase system due to power oscillation in the 2nd harmonic frequency [8], [9]. This power oscillation causes dc-link voltage fluctuation and reduces the MPPT algorithm efficiency when PV modules are connected directly to the inverter DC-link.

In general, PV inverters are connected to PCC through passive filters to suppress the harmonic components produced during the switching process. L filters are an attractive solution due to their simple implementation [10]. However, in practice, the connection through LCL filters present a small cost-benefit ratio, due to the smaller volume of the LCL filters, considering similar

2

attenuation capacity. However, LCL filters can insert resonances into the power system. Resonances can be damped through passive elements, i.e., adding a resistor r_d in series with the filter capacitor, or through active damping techniques [11], [12], [13].
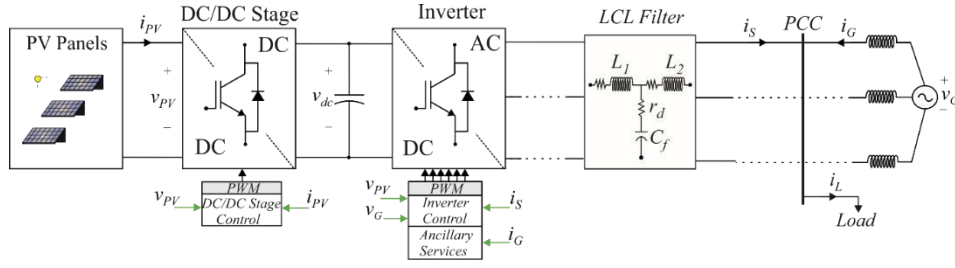
Fig. 2. Generic scheme of the grid-connected photovoltaic system for single-phase and three-phase applications

2.1. Solar Panel Modelling

The solar cells are the devices responsible for photovoltaic conversion, This structure can be represented as a diode with p-n junction exposed to sunlight [14]. Each cell can generate a power ranging from about 1 W to 2 W. Thereby, in practical and commercial applications, solar cells are connected in series or parallel associations and form modules.

There are several mathematical models used to represent the PV panel behavior. Fig. 3 shows the electrical equivalent circuit considering a single diode. In this model, the current from the solar panel terminals (I) can be represented by [15], [14]:

$$I = I_{pv} - I_0 \left(e^{\frac{V + R_S I}{V_t a}} - 1 \right) - \frac{V + R_s I}{R_p}. \tag{1}$$
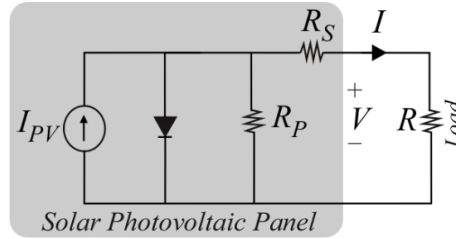
Fig. 3. Electrical model of Solar panel.

I_{pv} is the current generated by the incidence of sunlight, I_0 is the leakage current of the diode, a is the diode ideality constant and V_t is the panel thermal voltage [15], [17]. The equivalent series resistance (R_S) and the equivalent parallel resistance R_P depends mainly on the PV panel manufacture method and can be found by algorithms as presented in [15].

It is important to highlight that the simple and efficiency algorithm method presented in [15] to determine the PV panel parameters is well accepted in the literature. However, the complex dependency of these parameters in relation to temperature and irradiance is still an interesting research issue. Reference [18] approaches a complex strategy to obtain an I-V curve of a PV panel based on the irradiance and temperature effects. More complex models considering more diodes, representing the recombination effect of carries are also used in power electronic studies [16].

2.2. Maximum Power Point Tracking (MPPT)

PV cells present low efficiency in electricity generation if compared to other sources of electric energy generation. For example, in 1998, the conversion efficiency of solar irradiance in useful electricity through monocrystalline silicon solar cells improved from 18 % to 24 % [19]. Despite several technological advances, the efficiency of these PV cell types have halted at around 24 % [20]. There are new and more efficient PV cell technologies, such as GaInP/GaAs multijunction. However, these devices are more expensive than silicon cells [20].

For this reason, the maximum power extraction is an important issue to ensure the highest possible efficiency of the solar panel. This goal is achieved through the MPPT algorithms that track the PV panel voltage, keeping the PV panel power around the MPP.

Due to low algorithm complexity and low computational power requirement, Perturbation and Observation (P&O) is the most traditional MPPT method. This algorithm periodically increments or decrements the solar array voltage and compares the output power with the previous value. If the delivered power is increased, the solar array voltage perturbation will continue in the same direction. When the supplied power starts to decrease, the system reaches MPP and the P&O algorithm output oscillates around it [21], [22]. Other traditional MPPT algorithm is the incremental conductance based method, which is a specific implementation of the P&O algorithm [23].

However, in cases of rapidly changing atmospheric conditions, the P&O algorithm can track wrong direction in relation to the MPP, which may reduce efficiency. This can happen when power variation, due to change in the solar irradiance, is higher than that caused by the algorithm action itself. Thereby, the algorithm interprets the power variation only as an effect of its own action [24]. Hence, variations of the P&O method are proposed in literature, in order to solve problems caused by the rapidly changing in irradiance, such as: Modified P&O method (MP&O) [25] and the dP-P&O method [24], [26].

2.3. Dc/dc Stage Based on Boost Converter

The use of dc/dc stage is recommended in single-phase applications, due to the voltage oscillation of two times the line frequency in the inverter dc-link. Reference [8], [9] approaches a boost converter in the dc/dc stage with a voltage control loop, Reference [27] use the buck converter and presents a control modelling.

The DC/DC control loop is shown in Fig. 6 (a) [5], [27], [28]. The boost converter control consists of an outer loop responsible for controlling the solar array output voltage (v_{pv}) and an inner loop tuned to regulate the boost converter inductor current, as show in Fig. 4. Some works use only the voltage control in the dc/dc stage [8], [9]. On the other hand, controlling the solar array output voltage through the inner loop inductor current can eliminate current overshoots [27].
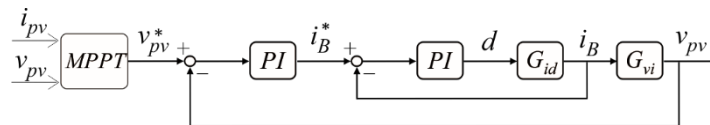
Fig. 4. Closed-loop model of the boost converter control.

Before the boost converter modelling, the PV array should be linearized around the nominal operation point. Therefore, the solar array can be represented by a linear circuit composed by a voltage source (V_{eq}) and equivalent series resistance (R_{eq}) [27]. The inverter dc-link can be represented by a voltage source. Thus, the small signal model is applied to achieve the transfer function of this system. Considering that "$\bar{v}$" refers to the average value within a period of

4

converter switching, uppercase letters "V_{eq} refer to the dc steady state value and the small signal disturbance represented by the "$\tilde{v}$" notation.
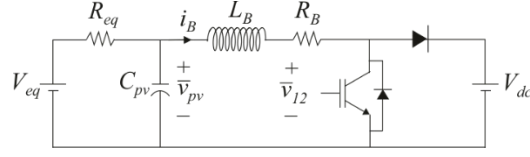
Fig. 5. Boost converter with PV array linear model.

The circuit shown in Fig. 5, leads to the achievement of the following equations:

$$\frac{V_{eq} - \bar{v}_{pv}}{R_{eq}} - C_{pv}\frac{d\bar{v}_{pv}}{dt} - \bar{\imath}_B = 0, \tag{2}$$

$$\bar{v}_{pv} - L_B\frac{d\bar{\imath}_B}{dt} - \bar{\imath}_B R_B - \bar{v}_{12} = 0. \tag{3}$$

The small signal disturbances, are given by:

$$\begin{cases} \bar{v}_{pv} = V_{pv} + \tilde{v}_{pv} \\ \bar{\imath}_B = I_B + \tilde{\imath}_B \\ d = D + \tilde{d} \end{cases}, \tag{4}$$

where d is the converter duty cycle.

By replacing (4) in (2) and (3) and taking into account $\bar{v}_{12} = (1 - d)V_{dc}$, the inner and outer loop transfer functions are given, respectively, by the formulas:

$$G_{id}(s) = \frac{\tilde{\imath}_B(s)}{\tilde{d}(s)} = \frac{V_{dc}}{L_B s + R_B}, \tag{5}$$

$$G_{vi}(s) = \frac{\tilde{v}_{pv}(s)}{\tilde{\imath}_B(s)} = -\frac{R_{eq}}{R_{eq}C_{pv}s + 1}. \tag{6}$$

3. Ancillary Services Supplied by PV Systems

Reactive power injection is an important ancillary service performed by PV inverters. Thus, the use of the PV inverter current margin to provide reactive power for industrial machines, e.g., can reduce the reactive power consumption from the power system, thus reducing its losses and improving the system stability [4], [5], [6], [29]. Voltage regulation is another advantage achieved by the insertion of the reactive power control capability into the PV inverter [30], [31]. The control of the active and reactive power flow can assist the recovery of the PCC voltage during an overvoltage or sag phenomena [31].

Due to the importance of the reactive power control in PV inverters, some countries have included this service in their grid code (GC) requirements. For example, in several countries, PV systems are required to immediately cease power generation in the presence of a grid fault [32]. However, due to the high penetration level of the PV system into the main grid, an immediate interruption of power generation during a quick grid fault may cause much greater problems. For this reason, several countries have updated their GCs, including Japan [33], Germany [34], [35],

Spain [36] [32], Italy [37]. It has been discussed the insertion of low-voltage ride-through (LVRT) capability in PV inverters, to allow reactive current injection to support voltage recovery during a grid fault [32], [38].

High levels of harmonic currents are related with devices used in industrial motor starters, lamps, computers and thyristor-based converters, which increase power losses in the utility grid and reduce the grid power quality [39]. Thus, some works in the literature have proposed the use of PV inverters to compensate the harmonic currents generated by nonlinear loads [4], [5], [6]. This concept consists in the detection of harmonic load content and its addition to the inverter control strategy. Thus, it is possible to cancel or reduce the harmonic current injected into the main grid. This strategy allows the PV inverter to perform as an active power filter, improving the grid power quality index in terms of total harmonic distortion (THD) [40], [41], [42].

Another issue that has been discussed in GCs is the probable scenario wherein PV systems become the major source of the electricity generation system. This scenario may be real due to the unprecedent growth of this system in recent years [43]. The PV system usually presents an energy generation peak in a period of lower demand, if compared with other periods of the day [44]. Therefore, during high PV system generation and low demand scenario, it is possible to reverse power flow, and consequently, overvoltage in the low voltage feeders, due to their more resistive characteristic [45]. Aiming to solve this problem, some works have proposed to directly curtail the active power injection by the PV systems when the grid voltage reaches its upper voltage limit [45], [46], [8]. It implies that the PV system should be able to operate with controllable power generation.

The active power control also allows the PV inverters to contribute with the main-grid frequency regulation. Synchronous generators work in nominal frequency when power generation and load consumption are in a state of equilibrium. However, reduced grid frequency is observed when the system is operating above its generation capacity [47]. Thereby, some works have reported PV system application for grid frequency support [47], [48], [49]. In [47], it is addressed a brief review on frequency regulation methods applied to the PV system.

4. Control Schemes for PV Inverters with Reactive Power Injection and Harmonic Current Compensation

4.1. Single-Phase PV Inverters

In order to include in the PV inverters the capability to perform reactive injection and harmonic current compensation, additional sensor can be necessary, mainly if the compensation scheme is performing by current controllers. This is a relatively simple modification in the inverter scheme presented in Fig. 2, which can increase considerably the inverter performance.

For single-phase PV inverters, different control strategies can be addressed in different reference frames [5], [4] approach the control based in $\alpha\beta$ reference frame. In [50] its is approached the dq and $\alpha\beta$ reference frame for single-phase and three-phase PV inverters. Reference [51] approach the control loop for in abc coordinated for tree-phase system. Three strategies widely used to control a single-phase PV inverter with ancillary services are shown in Fig. 6. These control strategies are composed of outer loops, designed to control the dc-link voltage and the reactive power injected at the PCC, and inner loops to control the inverter current. The single-phase inverter has only one current component [50].

A control strategy in dq-reference frame is shown in Fig. 6 (a). In this configuration, the inverter current loop control is synchronized with the grid voltage. Thus, grid currents and voltages in fundamental frequency are converted into dc components [50], [9]. For this reason, dq-control strategies are generally associated with proportional-integral (PI) controllers, since these controllers have a satisfactory tracking capability of dc signals.

6

When current harmonic compensation is performed, the inverter reference current has one or more harmonic orders. In this case, PI controller can insert steady state error due its limited tracking capability for high frequencies [52]. Therefore, to overcome this drawback, resonant controllers (R) have been employed when harmonics are compensated by inverters [50], [9], [53]. The resonant controller provides a theoretical infinite gain at the resonant frequency and reduces the steady state error. However, one resonant controller needs to be designed for each compensated harmonic component. Therefore, it is used the proportional multi-resonant controller (PMR) [53].

In this topology, the inverter must be synchronized with the grid. The traditional synchronism structure is the method based on synchronous reference frame phase-locked loop (SRF-PLL) [54]. Other synchronization techniques have been proposed to improve the extraction of the voltage fundamental angle under distorted grid, such as PLL based on second order generalized integrator (SOGI-PLL) [10], [55].

The control strategy in $\alpha\beta$-reference frame is shown in Fig. 6(b). This strategy has less terms to be controlled in relation to dq-reference frame control strategy. However, one resonant controller is necessary for each compensated harmonic component. Moreover, such as in dq-reference frame, in the $\alpha\beta$ strategy, it is necessary to estimate the grid voltage phase angle, by means of a synchronization structure.

Finally, the dc-link squared voltage control based method can also be employed in single-phase system, thus eliminating the use of synchronization strategies such as SOGI-PLL, as shown in Fig. 6(c). In distorted grid voltage conditions, may be necessary to include the frequency-locked loop (FLL) to detect the fundamental component of the grid voltage. Thus, a frequency adaptability structure using a single algorithm is required [10]. In both active power (P) and reactive power (Q) references provided by the dc-link voltage control loop are used with the instantaneous power theory equation, for the single-phase system:

$$i_\alpha = \frac{2}{v_\alpha^2+v_\beta^2}\left(v_\alpha P + v_\beta Q\right), \tag{7}$$

where i_α is the inner loop current reference [50], [41].

In order to achieve harmonic current compensation, it is necessary a stage to detect the harmonic current content ($\tilde{\imath}_L$). The traditional methods are based on the instantaneous power theory [56] and conservative power theory [57]. The dq-control strategy has the advantage of allowing the compensation of two harmonics with just one resonant controller [58].

Table 1 shows a summary of the advantages of each control strategy approached in Fig. 6. In terms of number of current controllers Fig. 6 (a) requires 2 current controllers . The controller type and the presence of a PLL structure in power balance conditions are also compared. Finally, the resonant controller complexity under power balancing events is compared, where "+" means more resonant controllers must be inserted and "-" means less resonant controllers are needed, reducing de complexity.

Table 1: Comparison between the strategies addressed in **Fig.** 6.

	Controller Scheme (a)	Controller Scheme (b)	Controller Scheme (c)
Number of current controller	2	1	1
Controller type	PI, Multi-Resonant controllers	Proportional Multi-Resonant controllers	Proportional Multi-Resonant controllers
PLL in power balances conditions	yes	yes	no
Resonant Controller complexity under power balancing events	-	+	+
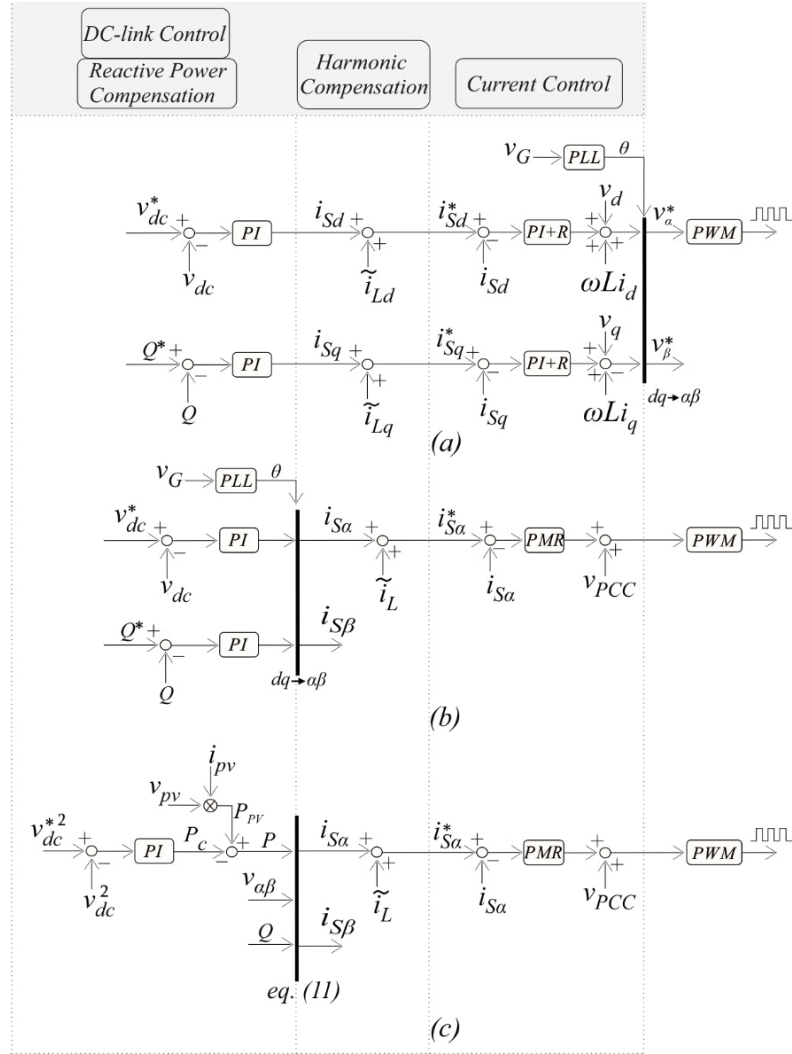
Fig. 6. Generic control schemes for single-phase multifunctional photovoltaic inverter: (a) Current control in dq-reference frame. (b) Current control in $\alpha\beta$-reference frame. (c) Current control in $\alpha\beta$-reference frame with v_{dc}^2 strategy for DC-link voltage control.

4.2. Three-Phase PV Inverters

Four control strategies widely used in the three-phase PV inverter are shown in Fig. 7. In all cases, the Space Vector Pulse Width Modulation (SVPWM) is the modulation strategy recommended. It provides output voltages with amplitudes higher than those generated by the conventional sinusoidal PWM strategy [59].

All four strategies have an MPPT algorithm to calculate the voltage reference for outer loops, designed to control the DC-link voltage and the reactive power injected at the PCC. The inner loops are responsible for controlling the inverter injected current. It must be highlighted that inner loop structures can be implemented at different reference frames.

A control strategy in the dq-reference frame is shown in Fig. 7 (a). Similar to the single-phase inverter control, in the dq-reference frame and equilibrated power system, it is possible to compensate two harmonic components with one resonant controller and reduce the control complexity. However, this approach includes extensive transformation and the current decoupling terms still present.

Considering other reference frames, those based on $\alpha\beta$ and abc-coordinate are constantly addressed in the literature [50], [9], [60], [51]. These control methods are shown in Fig. 7 (b) and

Fig. 7 (c), respectively. In comparison with abc reference-frame, the topology of control in $\alpha\beta$ is simpler, since it considers only two control variables.
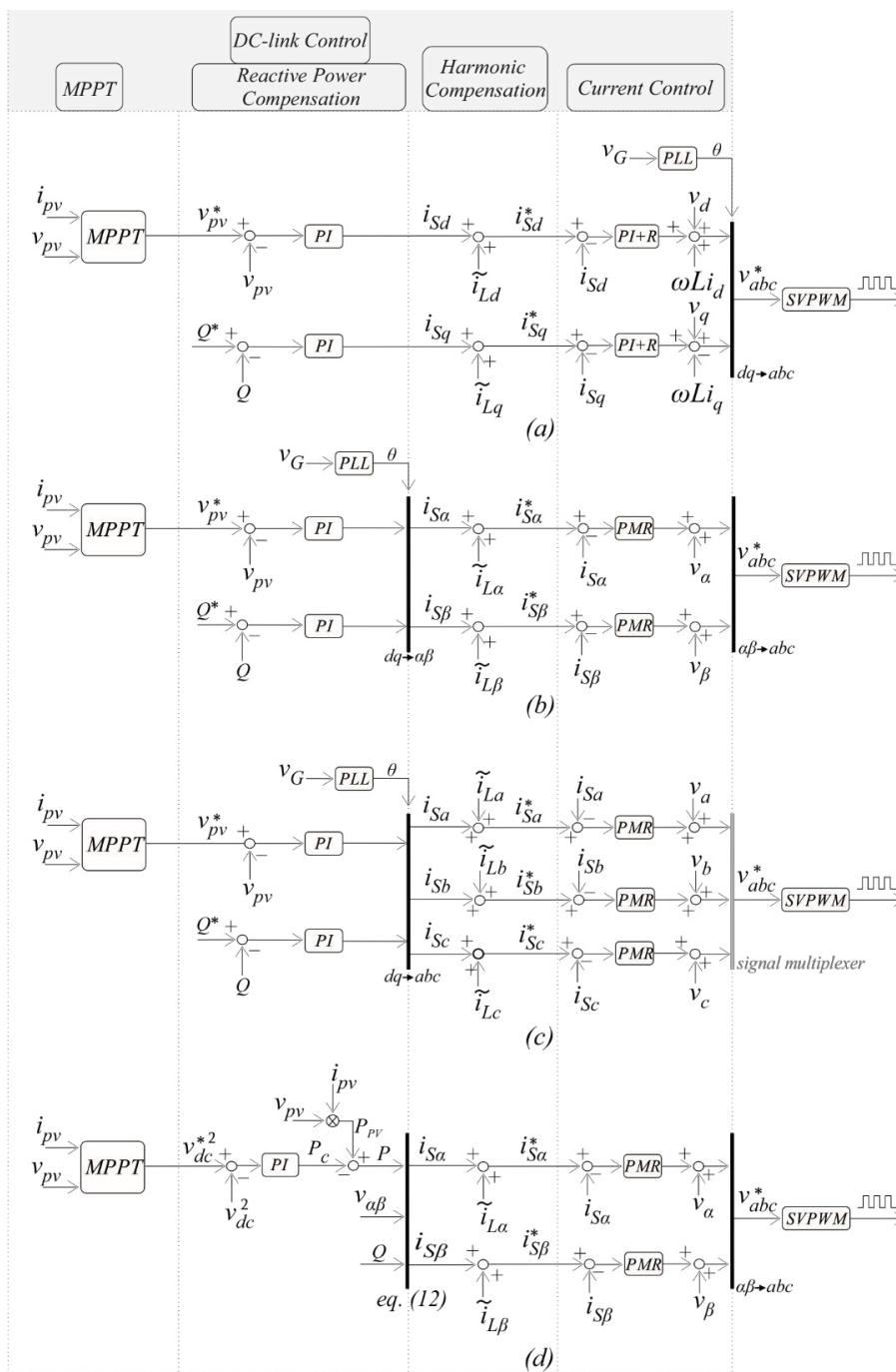
Fig. 7. Generic control schemes for three-phase multifunctional photovoltaic inverter. (a) Current control in dq-reference frame. (b) Current control in $\alpha\beta$-reference frame. (c) Current control in abc-reference frame. (d) Current control loop in $\alpha\beta$-reference frame with v_{dc}^2 strategy for DC-link voltage control.

All current control strategies are associated in cascade with dc-link voltage control or reactive power control. In all described cases, the grid phase angle must be estimated for the performance of Park's transformations. Another alternative method to regulate the dc-link voltage is presented in [6], which consists in controlling the dc-link squared voltage. The modelling of the outer loop is carried out from the storage energy in the dc-link capacitor. The active power reference is generated by the DC-link voltage control. Therefore, provided the reactive power reference, the equation of the instantaneous power theory, is given by [56], [61]:

$$\begin{bmatrix} i_\alpha \\ i_\beta \end{bmatrix} = \frac{1}{v_\alpha^2 + v_\beta^2} \begin{bmatrix} v_\alpha & v_\beta \\ v_\beta & -v_\alpha \end{bmatrix} \begin{bmatrix} P \\ Q \end{bmatrix}, \tag{8}$$

where i_α and i_β are the inner loop current reference. The v_{dc}^2 strategy can be applied in any reference frame. However, in $\alpha\beta$-reference frame, the synchronization techniques are unnecessary, which reduces the control complexity, as shown in Fig. 7 (d). It is worth highlighting that the reactive power is in open loop when the v_{dc}^2 control strategy is used and an error in the inner loop control can affect the injected reactive power dynamic. In three-phase inverters, the grid synchronization can be also performed using the traditional synchronous reference frame phase-locked loop (SRF-PLL) [54]. Other more advanced synchronization structures are PLL based on dual second order generalized integrator (DSOGI-PLL) [62] and PLL based on decoupled double synchronous reference frame (DDSRF-PLL) [63].

Considering a balanced three-phase system, the dq-control strategy has the advantage of allowing the compensation of two harmonics at $(6k \pm 1)\omega_f$, where $(k = 1, 2, ...)$, with just one resonant controller [58]. However, under unbalanced power condition, the number of resonant controllers can double in dq strategy in relation to the αβ control strategy. Table 2 shows a summary of the advantages of each control strategy addressed in Fig. 7 in terms of the same parameters approach in Table 1.

Table 2: Comparison between the strategies addressed in Fig. 7.

	Controller Scheme (a)	Controller Scheme (b)	Controller Scheme (c)	Controller Scheme (d)
Number of controlled currents	2	2	3	2
Type of applied controllers	PI, Multi-Resonant controllers	Proportional Multi-Resonant controllers	Proportional Multi-Resonant controllers	Proportional Multi-Resonant controllers
PLL in power balances conditions	yes	yes	yes	no
Resonant Controller complexity under power balancing events	-	+	+	+
Resonant Controller complexity under power unbalancing events	+	-	-	-

5. Inner loop Design

5.1. Inverter Current Controllers

In the literature, controllers are divided into two classes: on/off and based on pulse width modulator. The on/off method has simple implementation, and a hysteresis band has to be defined [64], [65], [66]. A disadvantage of this method is the fact that hysteresis current controllers have bad harmonic performance [64].

The controllers based on pulse width modulation involve both linear and nonlinear classes. The control based on passivity is a nonlinear controller frequently used in the literature [67], [52]. This controller is based on the energy concept and determines a relationship in which the plant stores less energy than it absorbs. This approach is valid for a wide range of operations and assures large signal stability.

On the other hand, linear controllers are the most used due to their high performance in tracking the signals, even when the signal has several frequencies. The conventional proportional-integral (PI) compensators fall into this category. Due to the infinite gain in the zero frequency, the application of this controller in the current control of the PV system is recommended when the inverter current reference is constant, i.e. when the inverter current control is based on

synchronous reference frame, as show in Fig. 6 (a)and Fig. 7 (a), without harmonic compensation [50], [9], [68]. Due to its limited bandwith, the current tracking capability of this controller is very poor. The transfer function of a PI controller if given by:

$$G_{PI}(s) = K_P^{PI} + \frac{K_i^{PI}}{s},$$

(9)

where K_P^{PI} is the proportional gain and K_i^{PI} is the integral gain

Therefore, by using the $\alpha\beta$ or abc control strategy or inserting the harmonic current compensation capability into the inverter control, other linear controllers are also widely used in the literature, such as proportional multi-resonant (PMR) controller [4], [50], [9], [53], [69], and repetitive controllers [50], [70], [71]. Differently from the resonant controllers, the resonance frequencies in repetitive controllers are achieved through feedback from the controller error delay. Thus, the number of resonances is related with the delay value [50], [70], [71].

The PMR controller is composed of a proportional controller and may have several resonant controllers tuned at each frequency present in the signal. The PMR transfer function is given by:

$$G_{PR}(s) = K_P^{PR} + \sum_{h=1}^{n} K_{ih}^{PR} \overbrace{\frac{s}{s^2 + \omega_h}}^{R_h(s)},$$

(10)

where K_P^{PR} is the proportional gain, h is the harmonic order ($h = 1,2,3...,n$), ω_h are resonant frequencies and K_{ih}^{PR} are the integral gains for each harmonic frequency. It is not recommended to tune a PMR controller through phase margin and crossover frequency analysis, as it is done with PI controllers. Therefore, the PMR tuning through critical point analysis in Nyquist diagram is addressed in [53].

The PMR controller has high gains at its resonant frequencies. Thereby, the terms $R_h(s)$ are responsible for tracking the current components at ω_h frequencies [53]. The Tustin with prewarping is the discretization method recommended for $R_h(s)$. This technique avoids the shift of the resonant frequency for which it was tuned. Thus, $R_h(z)$ is given by [72]:

$$G_{PR}(z) = \frac{sin(\omega_h T_s)}{2\omega_h} \frac{1 - z^{-2}}{1 - 2z^{-1} cos(\omega_h T_s) + z^{-2}}.$$

(11)

K_P^{PR} and K_{ih}^{PR} are adjusted in accordance with reference [30], which considers the crossover frequency of the controller and its relationship with the critical point on the Nyquist diagram. In order to compare the current tracking capability of PI and PMR controllers, it is considered the plant transfer function in z-domain given by [53]:

$$P_L(z) = \frac{\left(1 - e^{\frac{R_T T_s}{L_T}}\right) z^{-2}}{\left(1 - z^{-1} e^{\frac{R_T T_s}{T_f}}\right) R_T},$$

(12)

where T_s is the sampling frequency, L_T and R_T are the total inductance and total equivalent series resistance of the LCL filter, respectively. The single-phase control loop based on the v_{dc}^2 strategy for dc-link voltage control is used for comparing these controllers in time domain during the current harmonic compensation. The inverter reference current contains frequencies of $60\ Hz$ and $300\ Hz$. Therefore, two resonant controllers are required. The proportional gains from both controllers are identical. Thereby, these controllers have the same crossover frequency, as shown in Fig. 8. The PI integral gain is maintained six times greater than the integral gain of the PR

controller. Therefore, the results illustrating the capability of photovoltaic inverters to perform ancillary services are conducted using PR controllers.
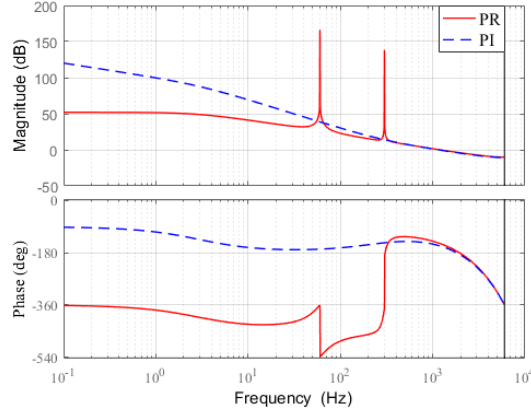
Fig. 8. PI and PR Bode diagram of the inverter open-loop transfer function.

5.2. Dynamic Saturation of the Inverter Current

Important issues arise when new capabilities are integrated in the PV inverter. In order to avoid damage and preserve the inverter lifetime and safety, the inverter current limit cannot be exceeded. Thereby, strategies for PV inverter current limitation are required during ancillary services support. The critical point is when harmonic current compensation is involved. When there are multiple frequencies in the current signal, analytical expressions for inverter current limitation are complex. Therefore, references [5], [6] have proposed hierarchical control strategies, in order to respect the inverter current margin.

These methods can be applied in all control strategies showed in Fig. 6 and Fig. 7. However, the loop with v_{dc}^2 strategy for dc-link voltage control has the advantage of already providing the active power reference to be injected by the inverter.

The reactive power saturation is the same for single and three-phase PV inverters, and is performed as shown in Fig. 9 (a), where S_m is the inverter rated power, P is the active power injected by the PV inverter and Q is the detected reactive power of the load. The saturation limit can be found by phasor calculation, as shown in Fig. 9 (b). The resultant power (S) of the phasor sum between P and Q should be contained in the circumference of radius S_m. Otherwise, the reactive compensation will be partial, ensuring that the inverter operation is below its rated current.

(a)   (b)
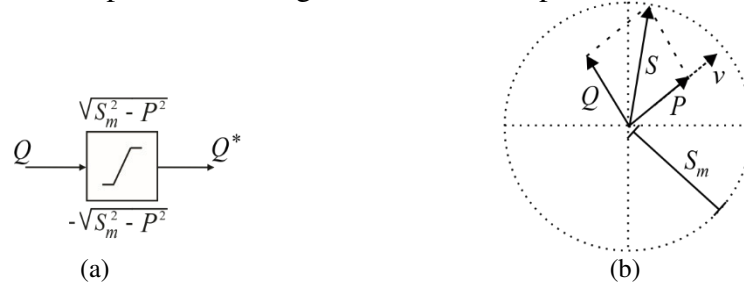
Fig. 9. (a) Reactive power saturation scheme. (b) Phasor calculation scheme to determine the saturation limit.

4.2.1 Harmonic Current Saturation in the Single-Phase System

The harmonic current saturation scheme for single-phase PV inverter is presented in Fig. 10, considering the control loop based on the $\alpha\beta$ coordinate shown in Fig. 6. The current ($i_{S\alpha}$) calculated by the outer loop is added to the load harmonic current ($\tilde{\imath}_L$), resulting in the inverter reference current ($i_{S\alpha}^*$). The maximum value of $i_{S\alpha}^*$ is detect by a peak detector algorithm and compared with the inverter rated current (I_m). An anti-windup PI controller, limited between 0 and 1, generates the dynamic factor (K) and determines if the compensation will be total or partial.
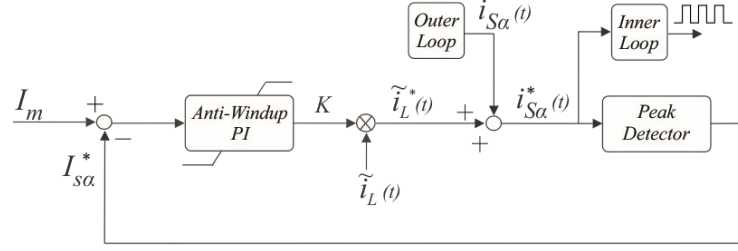
Fig. 10. Harmonic current saturation loop for single-phase inverter.

4.2.2 Harmonic Current Saturation in Three-Phase System

Harmonic current saturation scheme for the three-phase PV inverter is presented in Fig. 11. This strategy is similar to the single-phase scheme. However, it is performed on the inverter reference current in the abc coordinate. The instantaneous active current (i_{Sabc}) calculated by the outer loop is added to the load harmonic current ($\tilde{i}_{Labc}$), resulting in the inverter reference current (i^*_{Sabc}). Considering a balanced system, the maximum value of i^*_{Sa} is detect by a peak detector algorithm and compared with the inverter rated current (I_m). The anti-windup PI controller, limited between 0 and 1, generates the dynamic factor (K) and determines if the compensation will be total or partial.

For the current control loop based on the dq reference frame, the scheme of harmonic current saturation is similar to that shown in Fig. 11. The coordinate transformation is the only difference, i.e., the $\alpha\beta \rightarrow abc$ transformation is replaced by a $dq \rightarrow abc$ transformation.
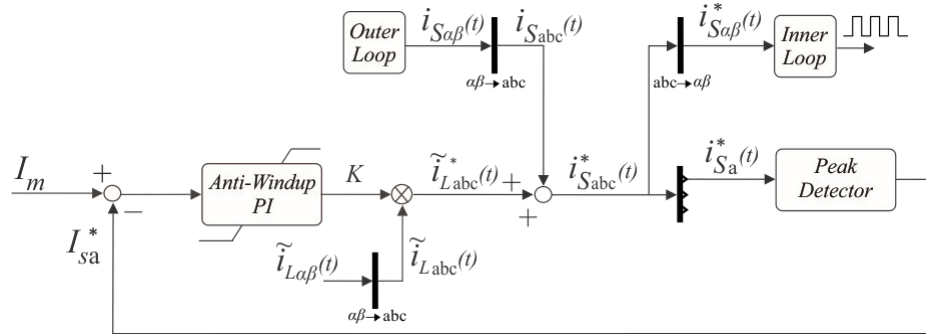
Fig. 11. Harmonic current saturation loop for three-phase inverter.

6. Case Studies

Case studies with simulation results are performed for single and three-phase PV system compensating reactive power and harmonic current to show the improvement of grid power quality. In both systems, the control strategy is based on the $\alpha\beta$ stationary reference frame with DC-link voltage control based on the v^2_{dc} strategy. In the single-phase system, the boost converter is used to regulate the PV array voltage with MPPT based on the conductance incremental algorithm. CPT is used in the single-phase case study and IPT is used in the three-phase case study. The PMR controller is adopted in the inner loop structure, and the inverter current limitation strategies are used to ensure that the inverter operates below its rated current. The parameters of both single and three-phase PV systems are shown in

Table 3 and Table 4, respectively.

Table 3: Parameters of the single-phase PV system case study.

Inverter and Grid Parameters	Value
Inverter switching frequency	$12\ kHz$
Fundamental frequency	$60\ Hz$
PCC voltage	$220\ V$
Grid Impedance	$1.30\ mH/48\ m\Omega$
V_{dc}^*	$390\ V$
DC-link PI controller gains	$K_P = 0.48\ W/V\ and\ K_i = 14\ W/V$
Current PMR controller gains	$K_P^{PR} = 7.5\ V/A\ and\ K_{ih}^{PR} = 2000\ V/A$
Boost Converter Parameters	Value
Boost converter switching frequency	$12\ kHz$
L_B/R_B	$0.8\ mH/10\ m\Omega$
C_{pv}	$500\ \mu F$
Outer loop PI control gains	$K_P^v = -0.75\ A/V\ and\ K_i^v = 132\ A/V$
Inner loop PI control gains	$K_P^i = 0.015\ 1/A\ and\ K_i^i = 0.19\ A^{-1}$
LCL Filter Parameters	Value
L_1	$0.5\ mH/9.42\ m\Omega$
L_2	$0.5\ mH/9.42\ m\Omega$
C_f	$6.33\ \mu F$
r_d	$1\ \Omega$
Harmonic Current Saturation Parameters	Value
Anti-Windup PI gain	$K_P^{AW} = 0.05\ 1/A\ and\ K_i^{AW} = 3\ 1/A$

Table 4: Parameters of the three-phase PV system case study.

Inverter and Grid Parameters	Value
Inverter frequency switching	$12\ kHz$
Fundamental frequency	$60\ Hz$
PCC voltage	$380\ V$
Grid Impedance	$2\ \mu H/19\ \mu\Omega$
DC-link PI controller gains	$K_P = 0.4\ W/V\ and\ K_i = 14\ W/V$
Current PMR controller gains	$K_P^{PR} = 7.5\ V/A\ and\ K_{ih}^{PR} = 2000\ V/A$
LCL Filter Parameters	Value
L_1	$0.5\ mH/9.42\ m\Omega$
L_2	$0.5\ mH/9.42\ m\Omega$
C_f	$6.33\ \mu F$
r_d	$1\ \Omega$
Harmonic Current Saturation Parameters	Value
Anti-Windup PI gain	$K_P^{AW} = 0.03\ 1/A\ and\ K_i^{AW} = 3\ 1/A$

The irradiance profile used in the case studies is shown in Fig. 12. Initially, the irradiance level is $850\ W/m^2$ and changes to $500\ W/m^2$ and $1000\ W/m^2$ at $1.5\ s$ and $2.2\ s$, respectively.
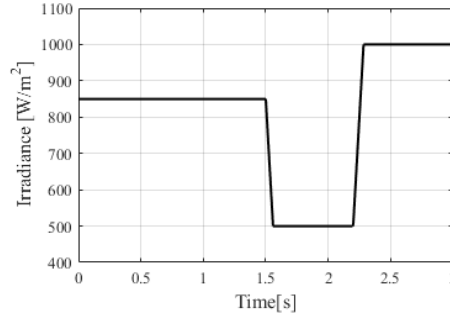
Fig. 12. Solar irradiance profile used in the study case of the single-phase and three-phase PV systems with ancillary services.

7. Simulation Results

7.1. Case I: Single-Phase PV System

The case study is composed of a PV plant consisting in 2 parallel strings with 6 panels of 250 W in series connections. The inverter rated power is 3 kW. The load connected at the PCC is a resistive-inductive load of 3.16 kVA with power factor of 0.95. There are also nonlinear loads represented by current sources emulating 5th and 7th harmonic current sources of 4 A and 3 A, respectively.

The dc-bus voltage profile of the solar array is illustrated in Fig. 13 (a), whose reference voltage is calculated by the MPPT algorithm. The boost inductor current is shown in Fig. 13 (b). The inverter dc-bus voltage is controlled in $390\,V$, as shown in Fig. 13 (c). The reactive power support is enabled at $0.5\,s$ and the harmonic current compensation is enabled at $0.8\,s$.
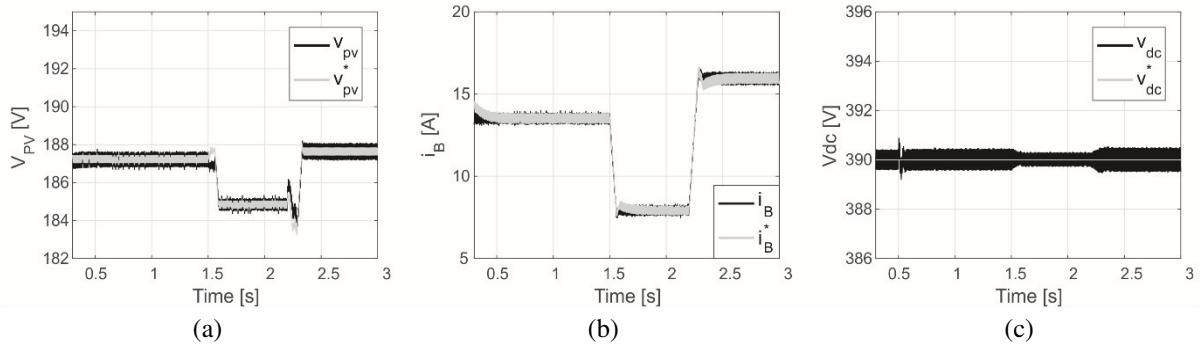
Fig. 13. (a) Dc-bus voltage profile. (b) Inductor current control of the boost converter. (c) Dc-link voltage profile.

When the solar irradiance is in $850\,W/m^2$ before $1,5\,s$, the inverter partially supplies the load active power, as observed in Fig. 14(a). At the same time interval, the PV inverter has current margin to supply all load reactive power, as shown in Fig. 14(b). When the harmonic current compensation is enabled at $0.8\,s$, the inverter has current margin to compensate 46.5 % of the load harmonic current, approximately, as shown in Fig. 15.

15
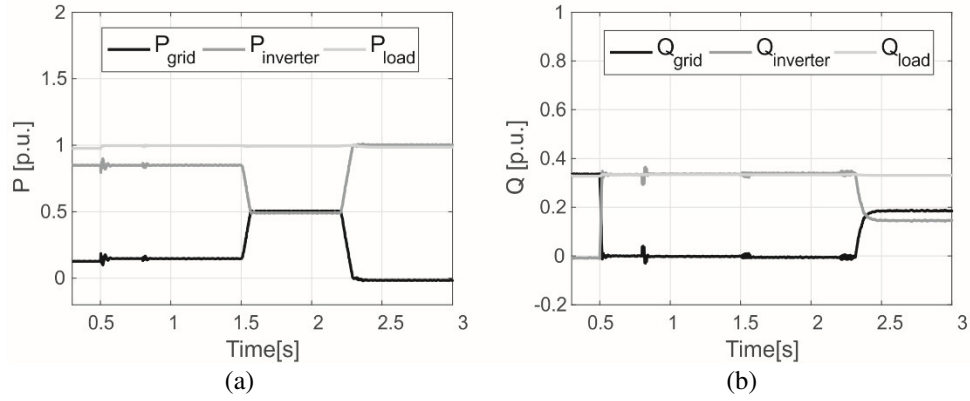
Fig. 14. Active power (P) and reactive power (Q) dynamic of the system with reactive power capability. (a) Active power of the system. (b) Reactive power of the system.
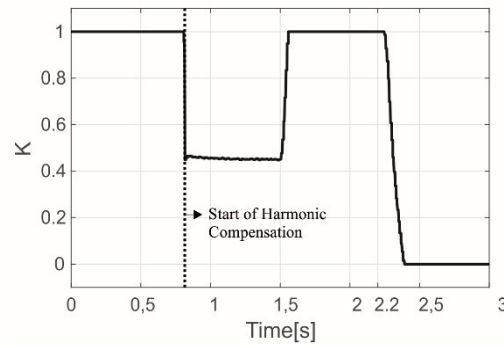
Fig. 15. K compensation factor of harmonic current.

The waveform details and the THD of the grid currents around $0.8\ s$ are shown in Fig. 16. Before $0.8\ s$, the inverter supplies almost all active power for the load, while the grid current has mostly harmonic distortions provided by the load. For this reason, the grid current THD is 178 %, as shown in Fig. 16 (a). When the partially harmonic compensation starts at $0.8\ s$, the harmonic distortions in the grid current are reduced. Thus, its THD decreases to 99 %, whereas the inverter current THD increases from 4.6 % to 13.6 %, as shown in Fig. 16 (b). As observed, the inverter current does not exceed the current limitation (I_{max}) at any moment. It is important to highlight that the load current THD is kept constant at 24,36 %.

Between 0.8 s and 1.5 s, the harmonic compensation is partial and the grid presents 5th and 7th harmonic current contents, as illustrated in *Fig. 17*(a). The 3rd harmonic component is present in *Fig. 17* due to the voltage oscillation in the inverter dc-link capacitor, which is a characteristic of single-phase systems, as already mentioned.
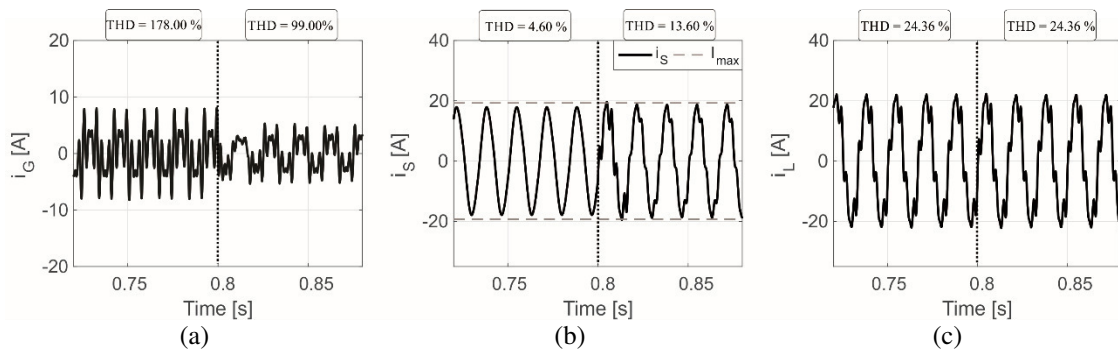
Fig. 16. System current details when harmonic current compensation is enabled at $0.8\ s$. (a) Grid current. (b) Inverter current. (c) Load current.

16
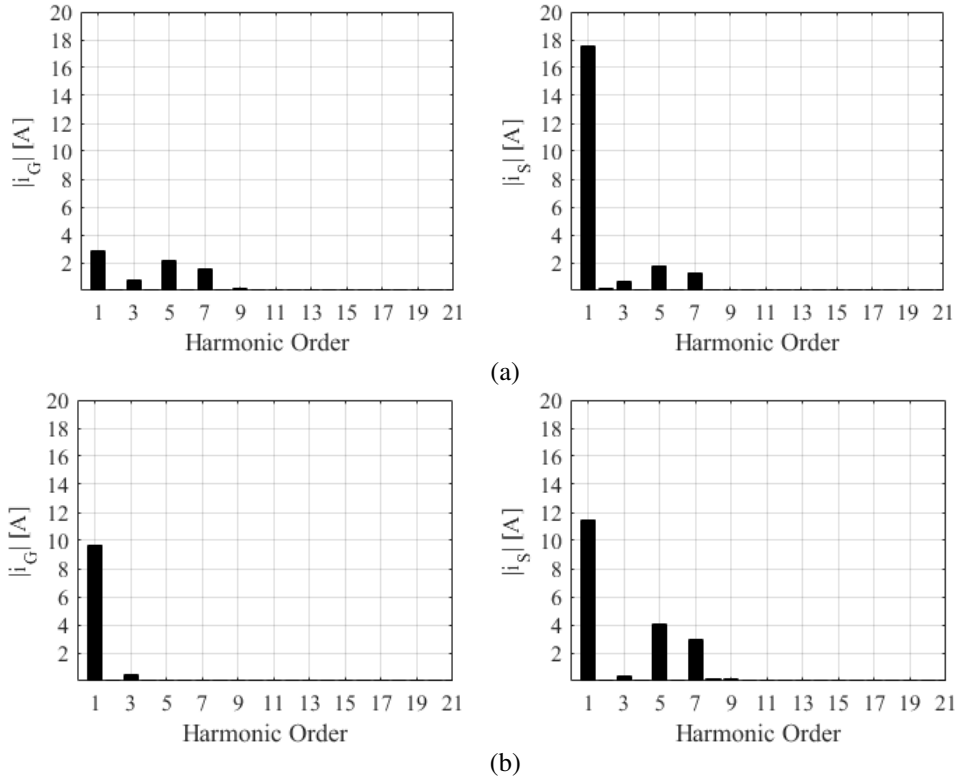
Fig. 17. Grid and inverter current spectra. (a) Between $0.8\ s$ and $1.5\ s$. (b) Between $1.5\ s$ and $2.2\ s$.

In $1.5\ s$, the irradiance decreases from $850\ W/m^2$ to $500\ W/m^2$. Thus, the PV inverter has margin to compensate 100% of the load reactive power and load harmonic current, as can be observed in Fig. 14 and Fig. 15, respectively. At this moment, the grid current THD decreases from 99% to 5.4%, as shown in Fig. 18(a). On the other hand, due to the increased K factor, the inverter current THD increases from 13,6% to 43,73%, as shown in Fig. 18 (b). The grid current increase after 1.5 s can be seen in Fig. 17. Between 1.5 s and 2.2 s, all harmonic content is compensated by the inverter and thus the 5th and 7th harmonic components are strongly reduced, as observed in Fig. 17(b).
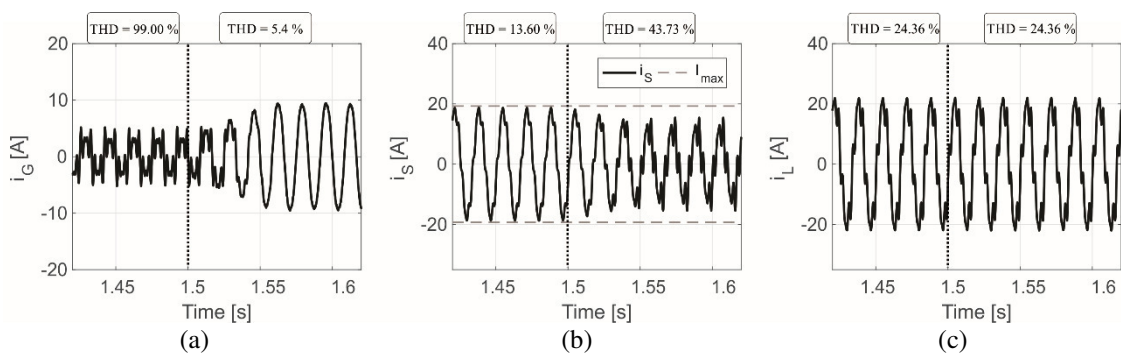
Fig. 18. System current details when solar irradiance changes from $850\ W/m^2$ to $500\ W/m^2$ at $1.5\ s$. (a) Grid current. (b) Inverter current. (c) Load current.

When the irradiance increases to $1000\ W/m^2$ at $2.2\ s$, the PV inverter has no margin to compensate the load reactive power and the load harmonic current, as observed in Fig. 14, respectively. At this moment, the grid current THD increases from 5,4 % to 140,81 %, as shown in Fig. 19(a). On the other hand, when K factor is null, the inverter current THD decreases from 43,73 % to 5 %.

17
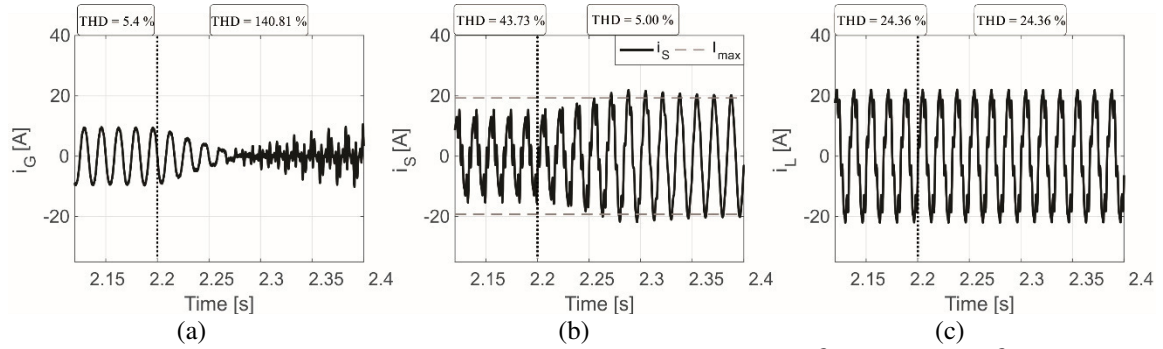
Fig. 19. System current details when solar irradiance changes from $500\ W/m^2$ to $1000\ W/m^2$ at $2.2\ s$. (a) Grid current. (b) Inverter current. (c) Load current.

Finally, this case study shows that a PV system with reactive power and harmonic current compensation capability can give support to the electrical power system when there is current margin for this purpose. These services are very significant for the PV system as well, since it remains below its nominal operation condition most of the day.

7.2. Case II: Three-phase PV System

The case study considering a three-phase PV system has a solar plant consisting of 4 parallel strings with 21 panels of 250 W in series connections. Therefore, the inverter rated power is 21 kW. The load connected to the PCC is a resistive-inductive load of 23.3 kVA with power factor of 0.9. There are also nonlinear loads represented by current sources emulating 5th and 7th harmonic of 6A and 3A, respectively.

The inverter dc-link dynamic is illustrated in Fig. 20. It is possible to observe the voltage variations calculated by the MPPT algorithm during the irradiance profile changing. Note the occurrence of perturbation in some moments due to the reactive power and harmonic current compensation, once these ancillary services are enabled at $0.5\ s$ and $0.8\ s$, respectively.
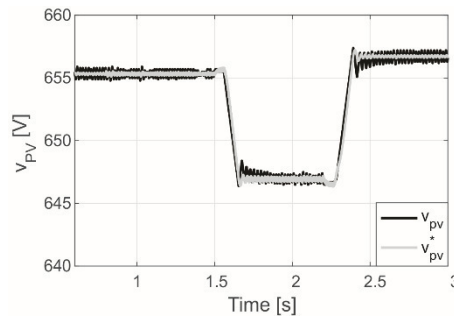
Fig. 20. Inverter DC-link dynamic.

When the solar irradiance is $850\ W/m^2$ before $1,5\ s$, the inverter partially supplies the load active power, as demonstrated in Fig. 21 (a). At the same time interval, the PV inverter has current margin to supply all load reactive power, as shown in Fig. 21 (b). However, when the harmonic current compensation is enabled at $0.8\ s$, the inverter has current margin to compensate 54 % of the load harmonic current, approximately, as shown in the K factor graphic in Fig. 22. The waveform details and the total harmonic distortion (THD) of the system currents around $0.8\ s$ are shown in Fig. 23. Before $0.8\ s$ the inverter supplies almost all load active power, while the grid current has basically harmonic distortions provided by the load. For this reason, the grid current THD is 99.03 %, as shown in Fig. 23 (a). When the partially harmonic compensation starts at $0.8\ s$, the harmonic distortions in the grid current are reduced. Thus, its THD decreases to 45.42 %, whereas the inverter current THD increases from 1.06 % to 8.25 %, as shown in Fig.

18

23 (b). Note that the inverter current does not exceed the current limitation (I_{max}) at any moment. It is important to highlight that the load current THD is kept constant at 13.29 % during the case study, as illustrated in Fig. 23 (c).

Due to irradiance decrease to 500 W/m^2 at 1.5 s, the PV inverter has margin to compensate 100% of the load reactive power and load harmonic current, as observed in Fig. 21 and Fig. 22, respectively. At this moment, the grid current THD decreases from 45.42 % to 2.24 %, as shown in Fig. 24 (a). On the other hand, the increased K factor increases the inverter current THD from 8.25 % to 21.63 %, as shown in Fig. 24 (b). Grid current increase after 1.5 s can be seen in spectra in Fig. 25. Between 0.8 s and 1.5 s, the harmonic compensation is partial and the 5th and 7th harmonic contents can be found in the grid current, as illustrated in Fig. 25 (a). Between 1.5 s and 2.2 s, all harmonic content is compensated by the inverter. Thus, the 5th and 7th harmonic components are strongly reduced, as observed in Fig. 25 (b).

(a)   (b)
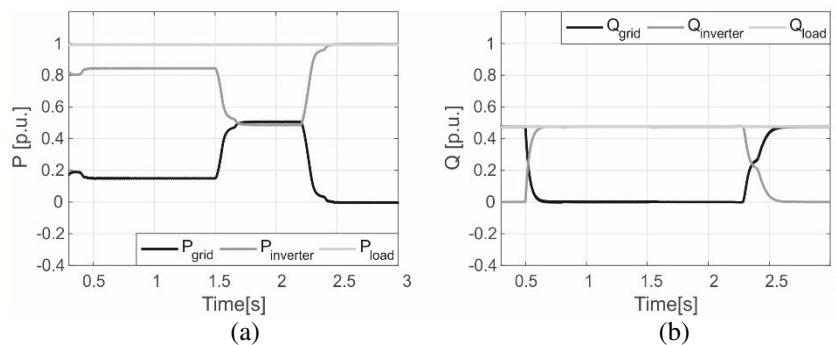
Fig. 21. Active power (P) and reactive power (Q) dynamic of the system with reactive power capability. (a) Active power of the system. (b) Reactive power of the system.
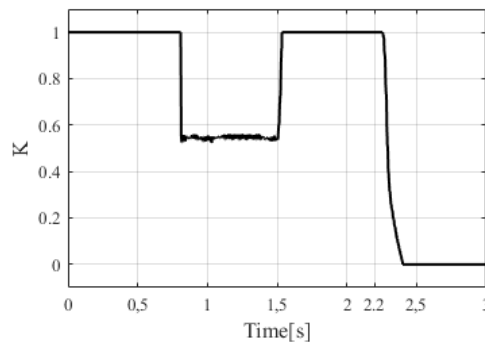
Fig. 22. K compensation factor of harmonic current.

(a)   (b)   (c)
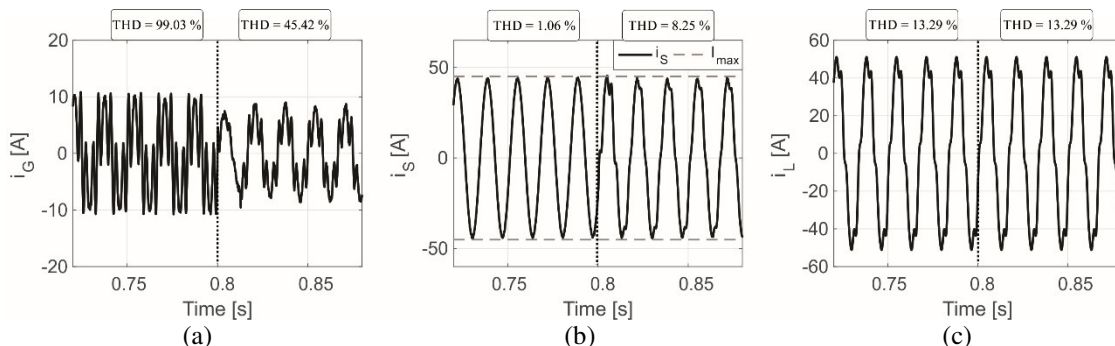
Fig. 23. System current details when harmonic current compensation is enabled at 0.8 s. (a) Grid current. (b) Inverter current. (c) Load current.
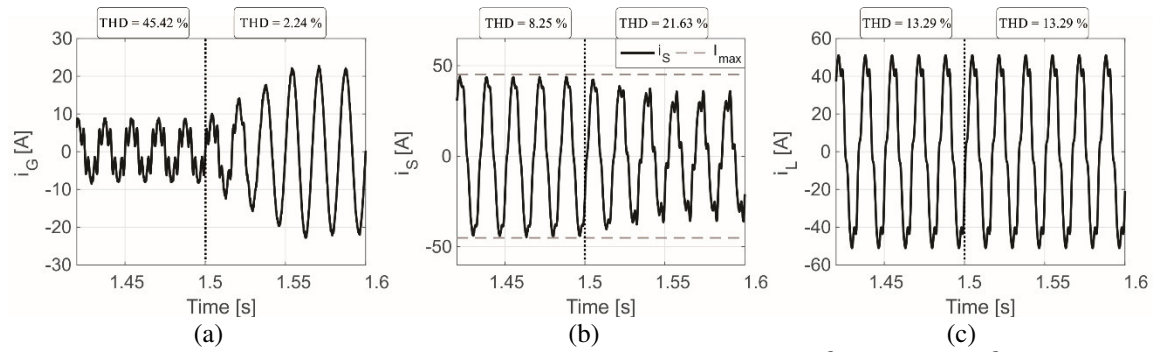
Fig. 24. System current details when solar irradiance changes from $850 \ W/m^2$ to $500 \ W/m^2$ at $1.5 \ s$. (a) Grid current. (b) Inverter current. (c) Load current.
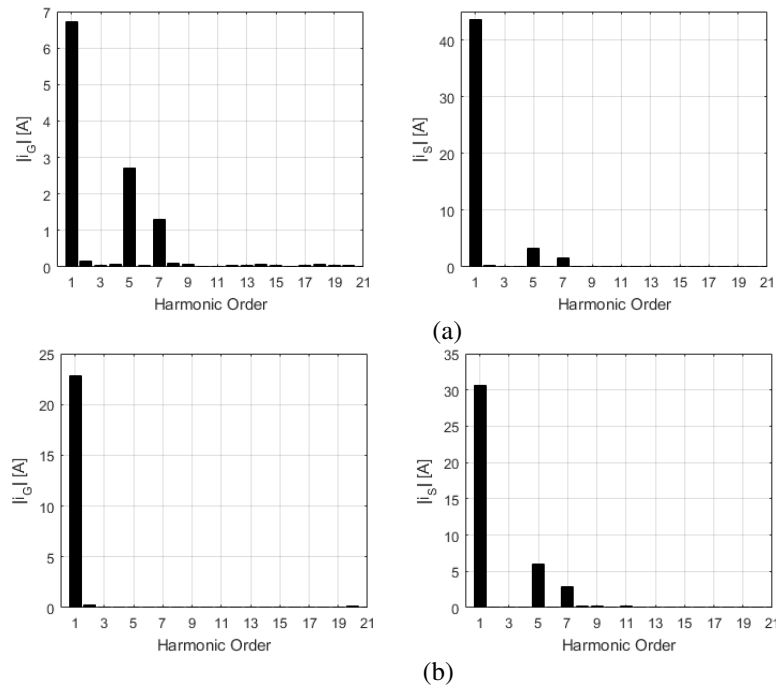
Fig. 25. Grid and inverter current spectra. (a) Between $0.8 \ s$ and $1.5 \ s$. (b) Between $1.5 \ s$ and $2.2 \ s$.

When the irradiance increases to $1000 \ W/m^2$ at $2.2 \ s$, the PV inverter has no margin to compensate the load reactive power and load harmonic current, as observed in Fig. 21 and Fig. 22, respectively. At this moment, the grid current THD increases from 2.24% to 31.11%, as shown in Fig. 26 (a). On the other hand, when the k factor is null, the inverter current THD decreases from 21.63% to 1.25%, as shown in Fig. 26 (b).
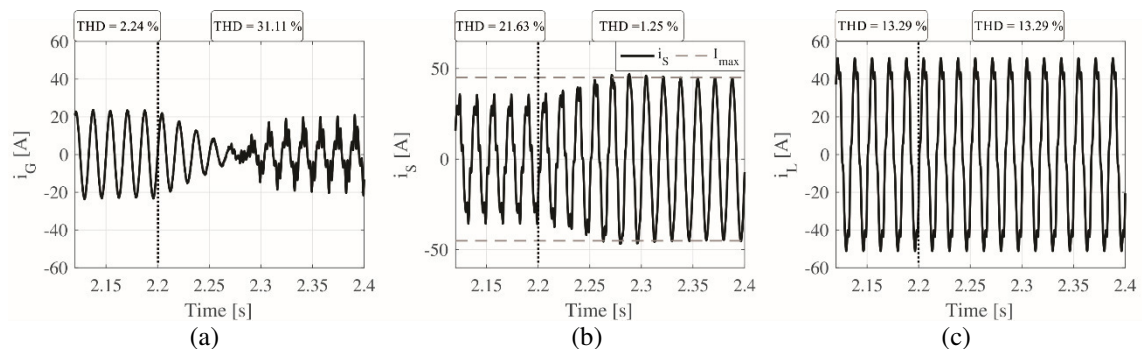
Fig. 26. System current details when solar irradiance changes from $500 \ W/m^2$ to $1000 \ W/m^2$ at $2.2 \ s$. (a) Grid current. (b) Inverter current. (c) Load current.

8. Conclusions

20

This paper has presented an overview about ancillary services, provided by single and three-phase PV systems, focusing on reactive power injection and harmonic current compensation. It is improved the inverter excess capacity, which is not used over the PV system daily operation. A generic topology of the grid-connected PV system with this ancillary service is presented, as well as several control structures based on different reference coordinates. It is mentioned the importance of the dc/dc stage for single-phase applications due to the voltage oscillation in the DC-link capacitor.

This study addressed the modelling of the main structures of the grid-connected PV system, including the solar panel, MPPT and current controllers. The PV inverter control strategy has several functions and must ensure that the inverter will operate below its rated current. Thus, strategies for inverter current limitation during the performance of auxiliary services are explored.

Lastly, two case studies are conducted to analyse the impact of ancillary service support on the PV system behavior. The results demonstrate that the PV inverter with reactive power support and harmonic current compensation capability can improve the power system quality, when there is current margin for this purpose. The results indicate that is possible to apply the control strategies addressed to perform ancillary services using both single-phase and three-phase systems.

References

[1] T. Kerekes, R. Teodorescu, M. Liserre, C. Klumpner and M. Sumner, "Evaluation of Three-Phase Transformerless Photovoltaic Inverter Topologies," *IEEE Trans. on Power Electronics,* vol. 24, no. 9, pp. 2202-2211, 09 2009.

[2] S. B. Kjaer, J. K. Pedersen and F. Blaabjerg, "A Review of Single-Phase Grid-Connected Inverters for Photovoltaic Modules," *IEEE Trans. Industry Applications,* vol. 41, no. 5, pp. 1292-1306, SEPTEMBER/OCTOBER 2005.

[3] J. Bonaldo, H. Morales Paredes and J. Antenor Pomilio, "Flexible operation of grid-tied single-phase power converter," *Brazilian Power Electronics Conference (COBEP),* pp. 987-992, Oct. 2013 27-31.

[4] J. Bonaldo, H. Morales Paredes and J. Antenor Pomilio, "Control of Single-Phase Power Converters Connected to Low-Voltage Distorted Power Systems With Variable Compensation Objectives," *IEEE Trans. Power Electron.,* vol. 31, no. 3, pp. 2039-2052, March 2016.

[5] H. Pereira, L. Xavier, A. Cupertino and V. Mendes, "Single-phase multifunctional inverter with dynamic saturation scheme for partial compensation of reactive power and harmonics," *17th European Conference on Power Electronics and Applications,* pp. 1-10, Sept. 2015.

[6] H. Pereira, R. Domingos, L. Xavier, A. Cupertino, V. Mendes and J. Paulino, "Adaptive saturation for a multifunctional three-phase photovoltaic inverter," *17th European Conference on Power Electronics and Applications ,* pp. 1-10, Sept. 2015.

[7] J. He, Y. W. Li and M. S. Munir, "A Flexible Harmonic Control Approach Through Voltage-Controlled DG–Grid Interfacing Converters," *IEEE Transactions on Industrial Electronics,* vol. 59, no. 1, pp. 444-455, Jan. 2012.

[8] A. Sangwongwanich, Y. Yang and F. Blaabjerg, "High-Performance Constant Power Generation in Grid-Connected PV Systems," *IEEE Trans. Power Electron.,* vol. 31, no. 3, pp. 1822-1825, 2016.

[9] F. Blaabjerg, R. Teodorescu, M. Liserre and A. V. Timbus, "Overview of Control and Grid Synchronization for Distributed Power Generation Systems," *IEEE Trans. Ind. Electron.,* vol. 53, no. 5, pp. 1398-1409, 2006.

[10] R. Teodorescu, M. Liserre and P. Rodriguez, Grid Converters for Photovoltaic and Wind Power Systems, Wiley-IEEE Press, 2011.

[11] R. Pena-Alzola, M. Liserre, F. Blaabjerg, M. Ordonez and Y. Yang, "LCL-Filter Design for Robust Active Damping in Grid-Connected Converters," *IEEE Trans. Ind. Informat.,* vol. 10, no. 4, pp. 2192-2203, 2014.

[12] M. Liserre, F. Blaabjerg and S. Hansen, "Design and control of an LCL-filter-based three-phase active rectifier. , 41, 1281–1291," *IEEE Trans. Ind. Appl.,* vol. 41, p. 1281–1291, 2005.

[13] W. Wu, Y. He, T. Tang and F. Blaabjerg, "A New Design Method for the Passive Damped LCL and LLCL Filter-Based Single-Phase Grid-Tied Inverter," *IEEE Trans. Ind. Electron.,* vol. 60, no. 10, pp. 4339-4350, 2013.

[14] H. S. Rauschenbach, Solar Cell Array Design Handbook, New York: Van Nostrand Reinhold, 1980.

[15] M. G. Villalva, J. R. Gazoli and E. R. Filho, "Comprehensive Approach to Modeling and Simulation of Photovoltaic Arrays," *IEEE Trans. Power Electron.,* vol. 24, no. 5, pp. 1198-1208, May 2009.

[16] J. A. Gow and C. D. Manning, "Development of a photovoltaic array model for use in power-electronics simulation studies," *IEE Proceedings - Electric Power Applications,* vol. 146, no. 2, pp. 193-200, Mar 1999.

[17] D. Sera, R. Teodorescu and P. Rodriguez, "PV panel model based on datasheet values," *IEEE International Symposium on Industrial Electronics,* pp. 2392-2396, 2007.

[18] M. Barukčić, V. Ćorluka and K. Miklošević, "The irradiance and Temperature dependent mathematical model for estimation of photovoltaic panel performances," *Energy Conversion and Management,* vol. 101, pp. 229-238, 2015.

[19] J. Zhao, A. Wang, M. A. Green and F. Ferrazza, "Novel 19.8% efficient honeycomb textured multicrystalline and 24.4% monocrystalline silicon solar cell," *Applied Physics Letters,* vol. 73, no. 14, pp. 1991-1993, 1998.

[20] M. A. Green, K. Emery, Y. Hishikawa, W. Warta and E. D. Dunlop, "Solar cell efficiency tables (version 47)," *Prog. Photovolt: Res. Appl.,* vol. 24, p. 3–11, 2016.

[21] K. Hussein, I. Muta, T. Hoshino and M. Osakada, "Maximum photovoltaic power tracking: an algorithm for rapidly changing atmospheric conditions," *Proc. Inst. Elect. Eng., Gener.,* vol. 142, no. 1, pp. 59-64, Jan 1995.

[22] M. A. Eltawil and Z. Zhao, " MPPT techniques for photovoltaic applications," *Renewable and Sustainable Energy Reviews,* vol. 25, pp. 793-813, September 2013.

[23] D. Sera, L. Mathe, T. Kerekes, S. V. Spataru and R. Teodorescu, "On the Perturb-and-Observe and Incremental Conductance MPPT Methods for PV Systems," *IEEE J. Photovolt.,* vol. 3, no. 3, pp. 1070-1078, July 2013.

[24] D. Sera, T. Kerekes, R. Teodorescu and F. Blaabjerg, "Improved MPPT method for rapidly changing environmental conditions," *IEEE International Symposium on Industrial Electronics,* vol. 2, pp. 1420-1425, 9-13 July 2006.

[25] C. Liu, B. Wu and R. Cheung, "Advanced Algorithm for MPPT Control of Photovoltaic Systems," *Canadian Solar Buildings Conference,* August 20-24, 2004.

[26] D. Sera, R. Teodorescu, J. Hantschel and M. Knoll, "Optimized Maximum Power Point Tracker for Fast-Changing Environmental Conditions," *IEEE Trans. Ind. Electron.,* vol. 55, no. 7, pp. 2629-2637, July 2008.

[27] M. G. Villalva, T. G. D. Siqueira and E. Ruppert, "Voltage regulation of photovoltaic arrays: small-signal analysis and control design," *IET Power Electronics,* vol. 3, no. 6, pp. 869-880, 2010.

[28] L. S. Xavier, J. H. d. Oliveira, A. F. Cupertino, V. F. Mendes and H. A. Pereira, "Saturation scheme for single-phase photovoltaic inverters in multifunctional operation," *IEEE 24th International Symposium on Industrial Electronics,* pp. 1392-1397, 2015.

[29] W. Libo, Z. Zhengming and L. Jianzheng, "A Single-Stage Three-Phase Grid-Connected Photovoltaic System With Modified MPPT Method and Reactive Power Compensation," *IEEE Trans. Energy Convers.,* vol. 22, no. 4, pp. 881-886, 2007.

[30] V. Miñambres-Marcos, M. Guerrero-Martínez, E. Romero-Cadaval and P. González-Castrillo, "Grid-connected photovoltaic power plants for helping node voltage regulation," *IET Renew. Power Gener.,* vol. 9, no. 3, pp. 236-244, 2015.

[31] B. K. Perera, P. Ciufo and S. Perera, "Point of common coupling (PCC) voltage control of a grid-connected solar photovoltaic (PV) system," *39th Annual Conf. of the IEEE Industrial Electronics Society (IECON),* 2013.

[32] Y. Yang, F. Blaabjerg and H. Wang, "Low-Voltage Ride-Through of Single-Phase Transformerless Photovoltaic Inverters," *IEEE Trans. Ind. Appl.,* vol. 50, no. 3, pp. 1942-1952, 2014.

[33] Y. Miyamoto, "Technology for high penetration residential PV systems," *Proc. of the 5th Int'l Conf. on Integration of Renewable and Distributed Energy Resources,* Dec. 2012.

[34] "Grid Code: High and Extra High Voltage," Bayreuth, Germany: E. ON GmbH, 2016.

[35] T. Stetz, F. Marten and M. Braun, "Improved Low Voltage Grid-Integration of Photovoltaic Systems in Germany," *IEEE Trans. Sustain. Energy,* vol. 4, no. 2, pp. 534-542, 2013.

[36] M. García-Gracia, N. El Halabi, H. Ajami and M. Comech, "Integrated Control Technique for Compliance of Solar Photovoltaic Installation Grid Codes," *IEEE Trans. Energy Convers.,* vol. 27, no. 3, pp. 792-798, 2012.

[37] "Reference technical rules for connecting users to the active and passive LV distribution companies of electricity," Comitato Elettrotecnico Italiano, Italy, 2011.

[38] Y. Yang, H. Wang and F. Blaabjerg, "Reactive Power Injection Strategies for Single-Phase Photovoltaic Systems Considering Grid Requirements," *IEEE Trans. Ind. Appl.,* vol. 50, no. 6, pp. 4065-4076, 2014.

[39] Z. Yao and L. Xiao, "Control of Single-Phase Grid-Connected Inverters With Nonlinear Loads," *IEEE Trans. Ind. Electron.,* vol. 60, no. 4, pp. 1384-1389, 2013.

[40] H. Akagi, "Control strategy and site selection of a shunt active filter for damping of harmonic propagation in power distribution systems," *IEEE Trans. Power Del.,* vol. 12, no. 1, p. 1997, 354-363.

[41] J. He, Y. W. Li, F. Blaabjerg and X. Wang, "Active Harmonic Filtering Using Current-Controlled, Grid-Connected DG Units With Closed-Loop Power Control," *IEEE Trans. Power Electron.,* vol. 29, no. 2, pp. 642-653, Feb. 2014.

[42] L. Asiminoaei, F. Blaabjerg, S. Hansen and P. ThØgersen, "Adaptive Compensation of Reactive Power With Shunt Active Power Filters," *IEEE Trans. Ind. Appl.,* vol. 44, no. 3, pp. 867-877, 2008.

[43] REN21, "Renewables 2016 Global Status Report," REN21 Secretariat, Paris, 2016.

[44] P. Denholm and R. M. Margolis, "Evaluating the limits of solar photovoltaics (PV) in traditional electric power systems," *Energy Policy,* vol. 35, no. 5, pp. 2852-2861, 2007.

[45] R. Tonkoski, L. A. C. Lopes and T. H. M. El-Fouly, "Coordinated Active Power Curtailment of Grid Connected PV Inverters for Overvoltage Prevention," *IEEE Trans. Sustain. Energy,* vol. 2, no. 2, pp. 139-147, 2011.

[46] C. H. Lin, W. L. Hsieh, C. S. Chen, C. T. Hsu and T. T. Ku, "Optimization of Photovoltaic Penetration in Distribution Systems Considering Annual Duration Curve of Solar Irradiation," *IEEE Trans. Power Syst.,* vol. 27, no. 2, pp. 1090-1097, 2002.

[47] P. Moutis, A. Vassilakis, A. Sampani and N. Hatziargyriou, "DC Switch Driven Active Power Output Control of Photovoltaic Inverters for the Provision of Frequency Regulation," *IEEE Trans. Sustain. Energy,* vol. 6, no. 4, pp. 1485-1493, Oct. 2015.

[48] H. Xin, Y. Liu, Z. Wang, D. Gan and T. Yang, "A New Frequency Regulation Strategy for Photovoltaic Systems Without Energy Storage," *IEEE Trans. Sustain. Energy,* vol. 4, no. 4, pp. 985-993, Oct. 2013.

[49] N. Kakimoto, S. Takayama, H. Satoh and K. Nakamura, "Power Modulation of Photovoltaic Generator for Frequency Control of Power System," *IEEE Trans. Energy Convers.,* vol. 24, no. 4, pp. 943-949, Dec. 2009.

[50] Y. Yang, K. Zhou and F. Blaabjerg, "Frequency Adaptability of Harmonics Controllers for Grid-Interfaced Converters," *International Journal of Control,* p. 1–12, 2015.

[51] L. Hassaine, E. OLias, J. Quintero and V. Salas, "Overview of power inverter topologies and control structures for grid connected photovoltaic systems," *Renewable and Sustainable Energy Reviews,* vol. 30, pp. 796-807, 2014.

[52] A. Cupertino, L. Carlette, F. Perez, J. Resende, S. Seleme and H. Pereira, "Use of control based on passivity to mitigate the harmonic distortion level of inverters," *IEEE PES Conf. on Innovative Smart Grid Technologies Latin America ,* pp. 1-7, April 2013.

[53] A. Yepes, F. Freijedo, O. Lopez and J. Doval-Gandoy, "Analysis and Design of Resonant Current Controllers for Voltage-Source Converters by Means of Nyquist Diagrams and Sensitivity Function," *IEEE Trans. Ind. Electron.,* vol. 58, no. 11, pp. 5231-5250, 2011.

[54] V. Kaura and V. Blasko, "Operation of a phase locked loop system under distorted utility conditions," *Applied Power Electronics Conference and Exposition,* pp. 703-708, 1996.

[55] M. Ciobotaru, R. Teodorescu and F. Blaabjerg, "A New Single-Phase PLL Structure Based on Second Order Generalized Integrator," *37th IEEE Power Electronics Specialists Conference ,* pp. 1-6, June 2006.

[56] H. Akagi, Y. Kanazawa and A. Nabae, "Instantaneous Reactive Power Compensators Comprising Switching Devices without Energy Storage Components," *IIEEE Trans. Ind. Appl.,* vol. IA20, no. 3, pp. 625-630, May 1984.

[57] P. Tenti, H. Paredes and P. Mattavelli, "Conservative Power Theory, a Framework to Approach Control and Accountability Issues in Smart Microgrids," *IEEE Trans. Power Electron.,* vol. 26, no. 3, pp. 664-673, 2011.

[58] R. I. Bojoi, G. Griva, V. Bostan, M. Guerriero, F. Farina and F. Profumo, "Current control strategy for power conditioners using sinusoidal signal integrators in synchronous reference frame," *IEEE Trans. Power Electron.,* vol. 20, no. 6, pp. 1402-1412, 2005.

[59] S. Buso and P. Mattavelli, "Digital Control in Power ElectronicsDigital Control in Power Electronics," in *Digital Control in Power Electronics*, Morgan & Claypool, 2006.

[60] N. D. Tuyen and G. Fujita, "PV-Active Power Filter Combination Supplies Power to Nonlinear Load and Compensates Utility Current," *IEEE Power Energy Technol. Syst. J.,* vol. 2, no. 1, pp. 32-42, 2015.

[61] H. Akagi, E. Watanabe and M. Aredes, "Instantaneous Power Theory and Applications to Power Conditioning," vol. 1, John Wiley & Sons, 2007.

[62] P. Rodriguez, R. Teodorescu, I. Candela, A. Timbus, M. Liserre and F. Blaabjerg, "New Positive-sequence Voltage Detector for Grid Synchronization of Power Converters under Faulty Grid Conditions," *37th IEEE Power Electronics Specialists Conf.,* pp. 1-7, June 2006.

[63] P. Rodriguez, J. Pou, J. Bergas, J. I. Candela, R. P. Burgos and D. Boroyevich, "Decoupled Double Synchronous Reference Frame PLL for Power Converters Control," *IEEE Trans. Power Electron.,* vol. 22, no. 2, pp. 584-592, 2007.

[64] H. Mao, X. Yang, Z. Chen and Z. Wang, "A Hysteresis Current Controller for Single-Phase Three-Level Voltage Source Inverters," *IEEE Trans. Power Electron.,* vol. 27, no. 7, pp. 3330-3339, 2012.

[65] C.-T. Pan and T.-Y. Chang, "An improved hysteresis current controller for reducing switching frequency," *IEEE Trans. Power Electron.,* vol. 9, no. 1, pp. 97-104, 1994.

[66] A. Shukla, A. Ghosh and A. Joshi, "Hysteresis Modulation of Multilevel Inverters," *IEEE Trans. Power Electron.,* vol. 26, no. 5, pp. 1396-1409, 2011.

[67] D. Jeltsema and J. M. A. Scherpen, "Tuning of passivity-preserving controllers for switched-mode power converters," *IEEE Trans. Autom. Control,* vol. 49, no. 8, pp. 1333-1344, 2004.

[68] E. Twining and D. G. Holmes, "Grid current regulation of a three-phase voltage source inverter with an LCL input filter," *IEEE Trans. Power Electron.,* vol. 18, no. 3, pp. 888-895, 203.

[69] M. Ciobotaru, R. Teodorescu and F. Blaabjerg, "Control of single-stage single-phase PV inverter," *European Conference on Power Electronics and Applications,* 2005.

[70] R. Teodorescu, F. Blaabjerg, M. Liserre and P. C. Loh, "Proportional-resonant controllers and filters for grid-connected voltage-source converters," *IEE Proceedings - Electric Power Applications,* vol. 153, no. 5, pp. 750-762, 2006.

[71] D. Chen, J. Zhang and Z. Qian, "An Improved Repetitive Control Scheme for Grid-Connected Inverter With Frequency-Adaptive Capability," *IEEE Trans. Ind. Electron,* vol. 60, no. 2, pp. 814-823, 2003.

[72] A. G. Yepes, F. D. Freijedo, J. Doval-Gandoy, Ó. López, J. Malvar and P. Fernandez-Comesaña, "Effects of Discretization Methods on the Performance of Resonant Controllers," *IEEE Trans. Power Electron.,* vol. 25, no. 7, pp. 1692-1712, 2010.